

High- T_c superconducting hydrides formed by LaH_{24} and YH_{24} cage structures as basic blocks.

Peng Song¹, Zhufeng Hou², Pedro Baptista de Castro^{3,4}, Kousuke Nakano^{1,5}, Kenta Hongo⁶, Yoshihiko Takano^{3,4}, Ryo Maezono¹

¹*School of Information Science, JAIST,
Asahidai 1-1, Nomi, Ishikawa 923-1292, Japan*

²*State Key Laboratory of Structural Chemistry,
Fujian Institute of Research on the Structure of Matter,
Chinese Academy of Sciences, Fuzhou 350002, China*

³*National Institute for Materials Science,
1-2-1 Sengen, Tsukuba, Ibaraki 305-0047, Japan*

⁴*University of Tsukuba, 1-1-1 Tennodai,
Tsukuba, Ibaraki 305-8577, Japan*

⁵*International School for Advanced Studies (SISSA),
Via Bonomea 265, 34136, Trieste, Italy*

⁶*Research Center for Advanced Computing Infrastructure,
JAIST, Asahidai 1-1, Nomi, Ishikawa 923-1292, Japan*

(Dated: February 17, 2022)

Based on recent studies regarding high-temperature (high- T_c) La-Y ternary hydrides (e.g., $P\bar{1}$ - $\text{La}_2\text{YH}_{12}$, $Pm\bar{3}m$ - LaYH_{12} , and $Pm\bar{3}m$ - $(\text{La},\text{Y})\text{H}_{10}$ with a maximum $T_c \sim 253$ K), we examined the phase and structural stabilities of the $(\text{LaH}_6)(\text{YH}_6)_y$ series as high- T_c ternary hydride compositions using a genetic algorithm and *ab initio* calculations. Our evaluation showed that the $Pm\bar{3}m$ - LaYH_{12} reported in the previous study was unstable during decomposition into $R\bar{3}c$ - $\text{LaH}_6 + Im\bar{3}m$ - YH_6 . We also discovered new crystal structures, namely $Cmmm$ - LaYH_{12} ($y = 1$), $R\bar{3}c$ - LaYH_{12} ($y = 1$), $Cmmm$ - $\text{LaY}_3\text{H}_{24}$ ($y = 3$), and $R\bar{3}$ - $\text{LaY}_3\text{H}_{24}$ ($y = 3$), showing stability against such decomposition. While $R\bar{3}c$ ($y = 1$) and $R\bar{3}$ ($y = 3$) did not exhibit superconductivity owing to the extremely low density of states at the Fermi level, $Cmmm$ phases exhibited a T_c of approximately 140 K at around 200 GPa owing to the extremely high electron-phonon coupling constant ($\lambda = 1.876$ for LaYH_{12}). By the twice longer stacking for $Cmmm$ - $\text{LaY}_3\text{H}_{24}$, the coupling constant increased owing to the chemical pressure of Y, leading to a slightly increased T_c .

I. INTRODUCTION

Metal hydrides have always been considered ideal candidates for high-temperature (high- T_c) superconductors owing to their ultrahigh phonon vibration frequency. [1, 2] However, realizing superconductivity by keeping them under the metallicity gradient often requires extremely high pressures. [1–6] Therefore, theoretical simulations play an extremely important role in search for novel hydride superconductors. [7–9] Through theoretical simulations, almost all the predictions for binary hydrides have been completed, and studies have successfully predicted the room-temperature superconductivity of YH_{10} . [10, 11] The successful prediction of room-temperature superconductivity in ternary $\text{Li}_2\text{MgH}_{16}$ [12] and the experimental discovery of room-temperature superconductivity in the C–S–H system [13] have pushed research on superconducting ternary hydrides system to a climax.

However, owing to the diversity of ternary hydrides, the search for new high- T_c superconductors appears very slow, and only 10 ~ 20 potential superconducting hydrides have been identified. [12–32] From the information obtained regarding binary superconductors, the crystal structure signif-

icantly influences the T_c . For example, some ultrahigh- T_c superconductors often appear in cubic systems such as ($Fm\bar{3}m$ - YH_{10} , $Fm\bar{3}m$ - LaH_{10} , and $Im\bar{3}m$ - H_3S , among others. [10, 33, 34] However, in ternary hydrides, the stability of the cubic structure is very poor, and many ternary systems may exhibit phase decomposition relative to binary hydrides. For example, CSH_7 , [28] is stable relative to C, S, and H, but not to binary hydrides CH_4 [35] and H_3S [34], possibly leading to phase decomposition. Owing to phase decomposition, it is highly unlikely that these compounds can be synthesized experimentally. Therefore, it is extremely important to ensure their stability relative to the constituent elements and binary materials for predicting ternary hydrides.

For searching ternary hydrides, there are two major approaches aiming at obtaining a high T_c , one focusing on SH_x doped with La, Se, Te, and Cl *etc.*, [19, 36–38] and the other on La- or Y-hydrides doped with metallic elements such as CaYH_{12} , CaMgH_{12} , KScH_{12} , and LaKH_{12} . [19, 39–41] With no significant improvement in T_c observed so far in the latter approach, the required pressure to realize superconductivity in these materials is considerably reduced, thereby providing the possibility of their experimental synthesis. Experiments in-

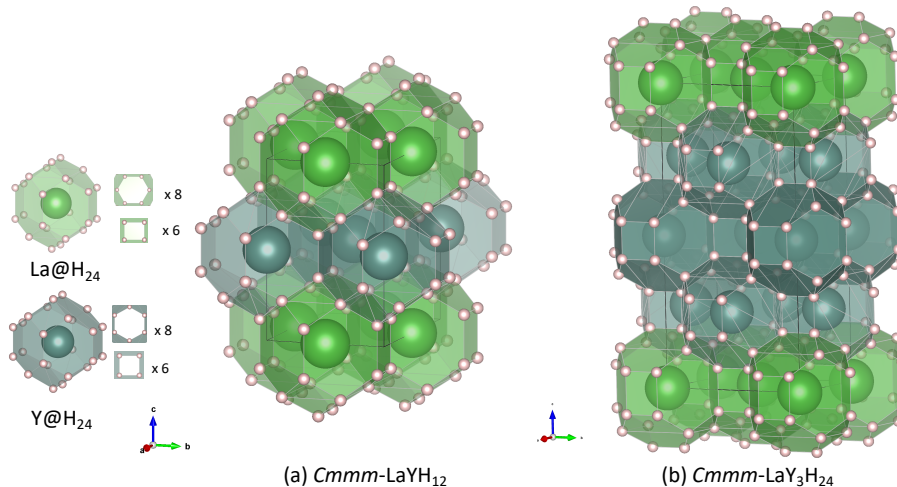


FIG. 1. Clathrate structure of LaYH_{12} (left panel, at 200 GPa) and $\text{LaY}_3\text{H}_{24}$ (right panel, at 180 GPa) with $Cmmm$, consisting of La-centered H_{24} cages and Y-centered H_{24} cages. Each H_{24} cage is surrounded by six squares and eight hexagons.

volving the La–Y–H system report high- T_c superconductivity in $(\text{La},\text{Y})\text{H}_{10}$. [42]

Based on these experiments, theoretical predictions of superconductivity in LaYH_{12} , $\text{La}_2\text{YH}_{18}$, $\text{La}_4\text{YH}_{30}$ etc. have been also reported. [42] These compositions are referred to as composites of $(\text{LaH}_6)_x + \text{YH}_6$. The symmetry of their predicted structures is considerably low mainly being $P\bar{1}$ with highest mostly $Pm\bar{3}m$ for LaYH_{12} . Examining its decomposition enthalpy revealed that the structure may exhibit phase decomposition under high pressure toward $R\bar{3}c\text{-LaH}_6 + Im\bar{3}m\text{-YH}_6$, being unlikely to be synthesized experimentally. [10, 11] We then determined whether LaYH_{12} has other structures stable against decomposition based on the USPEX fixed composition method. [7] Composition LaYH_{12} was also found in our machine learning search based on a gradient boosting tree [41], and it exhibited a high T_c . When searching more general forms, namely $(\text{LaH}_6)_x(\text{YH}_6)_y$, we restricted the range by fixing $x = 1$ because the preceding work has reported instability along the x -axis. Along the y -axis, we found $Cmmm\text{-LaYH}_{12}$ ($y = 1$) and $Cmmm\text{-LaY}_3\text{H}_{24}$ ($y = 3$) exhibiting a high $T_c \sim$ of 140 K. These compounds are formed through stacking of LaH_{24} and YH_{24} cages, as shown in Fig. 1. A slightly higher T_c for $Cmmm\text{-LaY}_3\text{H}_{24}$ compared to that for LaYH_{12} can be realized by enhancing the chemical pressure for Y through further stacking.

II. RESULTS

Fig. 2 shows the convex hull of our search for $\text{LaH}_6(\text{YH}_6)_x$ ($x = 1\text{-}4$) structures at 100, 200, and 300 GPa. LaYH_{12} ($x=1$) and $\text{LaY}_3\text{H}_{24}$ ($x=3$) are stable phases, whereas other $\text{LaY}_2\text{H}_{18}$ and $\text{LaY}_4\text{H}_{30}$ structures are likely to be decomposed at the abovementioned pressures. For the stable compositions, namely LaYH_{12} and $\text{LaY}_3\text{H}_{24}$, we compared their relative en-

thalpies with those of the candidate structures over the pressure range, as shown in Fig. 3. The plot for LaYH_{12} indicates that the $Pm\bar{3}m$ structure proposed recently [42] exhibits instability toward decomposition into binary compounds, namely $\text{YH}_6(Im\bar{3}m)$ and $\text{LaH}_6(R\bar{3}c)$.

For the entire pressure range, more stable structures are predicted as $R\bar{3}c \rightarrow Cmmm$ with the transition occurring at approximately $P = 140$ GPa, without instability toward decomposition. For $\text{LaY}_3\text{H}_{24}$, stable structures form as $R\bar{3}c \rightarrow Cmmm$, preventing its decomposition either to $\text{LaYH}_{12} + 2(\text{YH}_6)$ or $3(\text{YH}_6) + \text{LaH}_6$. As explained later, $R\bar{3}c\text{-LaYH}_{12}$ and $R\bar{3}\text{-LaY}_3\text{H}_{24}$ exhibit an extremely low density of states (DOS) at the Fermi level, $D(\epsilon_F)$, leading to a considerably low T_c . In contrast, $Cmmm$ compounds exhibit a higher T_c , and their structures are shown in Fig. 1. Detailed geometries for each structure are provided in Table II in the Supplemental Information (S.I.).

As observed in the Fig. 1, the structures are mostly clathrate structures formed by units with La@H_{24} and Y@H_{24} cage structures. Several other clathrate superconductors have been identified, [10–12, 21, 43–45] and hence it would be plausible for this structure to exhibit superconductivity. Different periodicities of the La- and Y-layers along the c -direction correspond to LaYH_{12} $[(\text{La}/\text{Y})(\text{La}/\text{Y})\cdots]$ and $\text{LaY}_3\text{H}_{24}$ $[(\text{La}/\text{Y}/\text{Y}/\text{Y})(\text{La}/\text{Y}/\text{Y}/\text{Y})\cdots]$, respectively.

Fig. 4 shows the phonon dispersions evaluated for the clathrate $Cmmm$ LaYH_{12} . We confirmed no imaginary modes, thus confirming its structural stability. The phonon dispersions for other structures are given in the S.I., confirming that all the candidates predicted from Fig. 3, namely $Cmmm\text{-LaYH}_{12}$, $Cmmm\text{-LaY}_3\text{H}_{24}$, $R\bar{3}c\text{-LaYH}_{12}$, and $R\bar{3}\text{-LaY}_3\text{H}_{24}$, have no imaginary modes. In contrast, $Pm\bar{3}m\text{-LaYH}_{12}$ proposed recently [42] exhibits imaginary modes, as shown in Fig. 5, consistent with the observations from Fig. 3 in terms

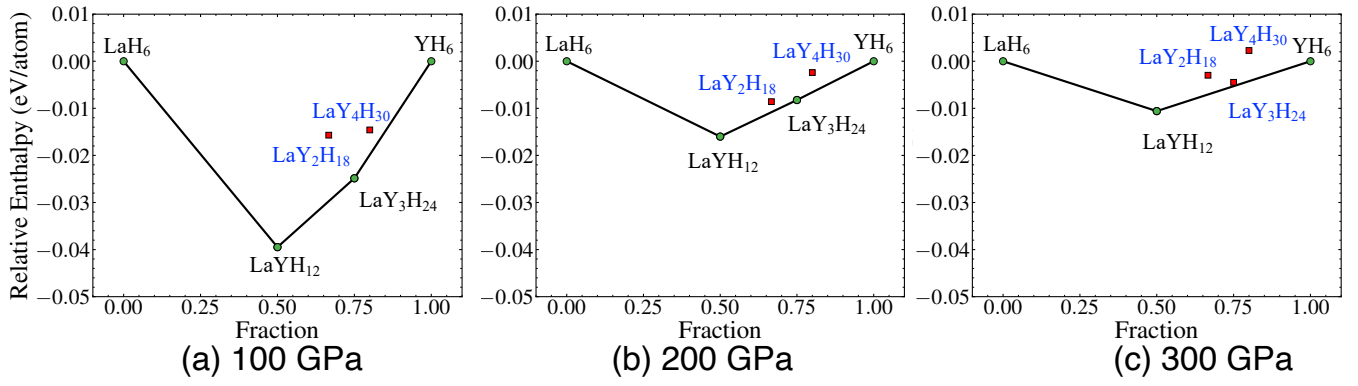


FIG. 2. Convex hull of La–Y–H at pressures of 100 GPa, 200 GPa, and 300 GPa.

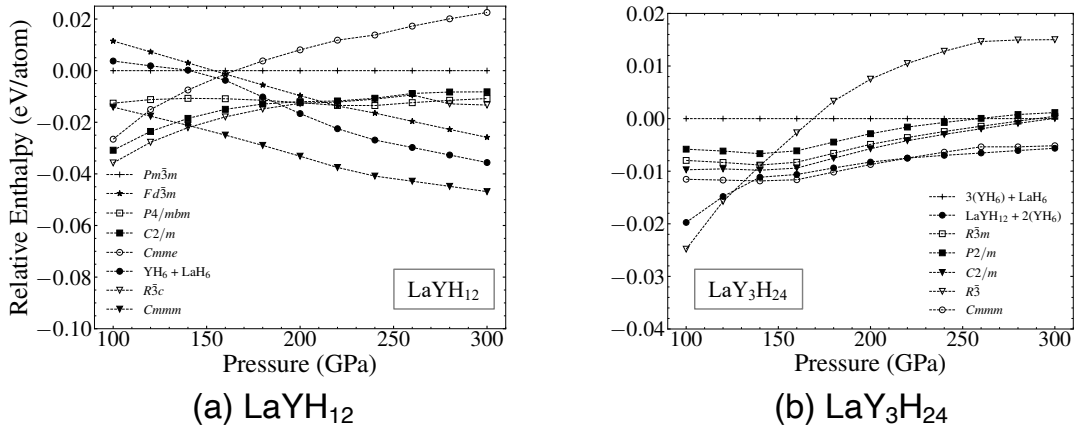


FIG. 3. Comparisons of candidate structure enthalpies for LaYH_{12} [panel (a)] and $\text{LaY}_3\text{H}_{24}$ [panel (b)]. Such structures giving higher values than those of ' $\text{YH}_6 + \text{LaH}_6$ ' (for the left panel), ' $3(\text{YH}_6) + \text{LaH}_6$ ' (for the right), and ' $\text{LaYH}_{12} + 2(\text{YH}_6)$ ' (for the right), are predicted to exhibit instability toward decomposition into these binary compounds.

of the instability.

Applying the Allen–Dynes formalism, [46–48] we estimated T_c as summarized in Table I. For LaYH_{12} , T_c is in the 130.6 ~ 140.55 [K] range, depending on the choice of parameter $\mu = 0.10 \sim 0.13$ for the Coulomb interaction. A slightly higher T_c realized for $\text{LaY}_3\text{H}_{24}$ is attributed to the higher $D(\varepsilon_F)$ due to the compressed chemical pressure for the Y-site with the (La/Y/Y/Y) stacking structure, compared to the (La/Y)(La/Y) periodicity.

III. DISCUSSIONS

As observed for $Fd\bar{3}m\text{-Li}_2\text{MgH}_{16}$, a room-temperature superconductor [12], the key factors for achieving a high T_c are its high DOS and high phonon frequency, which can be measured by λ and ω_{\log} , respectively. $\lambda = 2$ would be the typical criterion for realizing superconductivity ($\lambda = 3.35$ for $Fd\bar{3}m\text{-}$

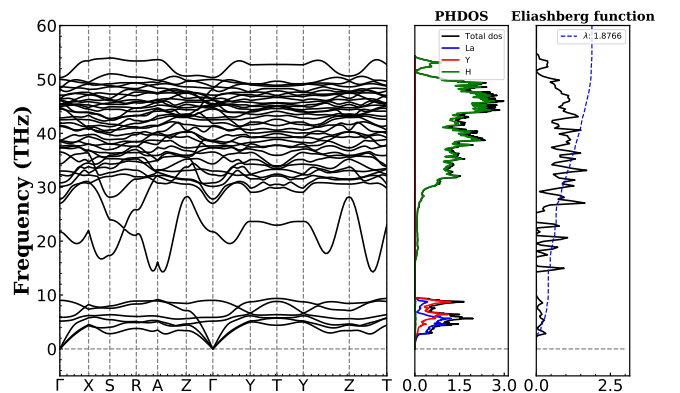


FIG. 4. Phonon dispersions, projected phonon densities of states, and Eliashberg spectral function for $Cmmm\text{-LaYH}_{12}$ clathrate at 200 GPa.

TABLE I. T_c (expressed in [K]) estimated using the Allen–Dynes formula through *ab initio* phonon calculations for LaYH_{12} and $\text{LaY}_3\text{H}_{24}$ at each pressure. λ and ω_{log} (expressed in [K]) are the parameters appearing in the formula. The values of $D(\epsilon_F)$ are expressed in [states/eV/atom].

	P [GPa]	λ	ω_{log}	$D(\epsilon_F)$	T_c ($\mu = 0.1 - 0.13$)
LaYH_{12}	200	1.876	1022.54	0.097	140.55 - 130.61
LaYH_{12}	250	1.618	1051.56	0.093	128.42 - 117.96
$\text{LaY}_3\text{H}_{24}$	180	2.452	891.49	0.100	145.31 - 137.11

$\text{Li}_2\text{MgH}_{16}$. [12]

In the S.I., we have provided the band structures and Fermi surfaces of $R\bar{3}c$ - LaYH_{12} and $R\bar{3}c$ - LaYH_{12} (Figs. 10 and 11). The Fermi surfaces and the DOS values on these surfaces are extremely small and are insufficient to achieve superconductivity.

In contrast, for the $Cmmm$ structure, sufficiently large Fermi surfaces and high DOS values lead to higher λ , thus resulting in superconductivity. Examining the phonon dispersions and Eliashberg spectral functions (Figs. 4, 8 and 9) reveals that higher λ values can be attributed to the contribution from the phonon branches appearing at higher ranges (> 10 THz), amounting to 96.2%. These branches are formed by the vibration of hydrogen atoms, whereas those at lower ranges (< 10 THz) by La and Y, negligibly contributing to λ .

Applying higher pressures (200 \rightarrow 250 GPa) to $Cmmm$ - $\text{LaY}_3\text{H}_{24}$ increases its phonon frequencies for the branches at higher ranges (> 10 THz), as observed in Figs. 4 and 8. This trend is reflected as the increased ω_{log} (Table I), contributing toward increasing the T_c . However, this trend disappears when the DOS (around 4.2%) decreases owing to the applied pressure, leading to a reduced λ value. This decrease is more dominant than the increase in ω_{log} , and hence the applied pressure eventually lowers the T_c , as observed in Table I.

The slightly higher T_c determined for $\text{LaY}_3\text{H}_{24}$ is attributed to the enhanced λ , as observed in Table I. In this case too, changes in ω_{log} and λ exhibit a cancelling relationship, causing only a slight increase in the T_c . Applying further pressure would mean increasing λ further for achieving a higher T_c ; however, according to the convex hull in our analysis, $Cmmm$ - $\text{LaY}_3\text{H}_{24}$ exhibits instability toward phase decomposition above 220 GPa.

$Pm\bar{3}m$ - LaYH_{12} exhibits a higher T_c (203 K at 180 GPa) [42] However, for this structure, the imaginary phonon modes appeared as shown in Fig. 5, implying structural instability at least within the extent of the harmonic approximation. As shown in Fig. 3, another structure, $Fd\bar{3}m$ - LaYH_{12} , is predicted to be more stable than $Pm\bar{3}m$. However, for both structures, the imaginary modes are found, without vanishing even on applying further pressure.

$Pm\bar{3}m$ - LaYH_{12} can be regarded as a compound based on the $Im\bar{3}m$ - YH_6 dimer with La substituting for one Y (Fig. 6). The $Im\bar{3}m$ - YH_6 actually appears as a stable structure in the convex-hull analysis given in Fig. 2. Our prediction, $Cmmm$ - LaYH_{12} , is actually a distorted structure of $Pm\bar{3}m$ - LaYH_{12} ,

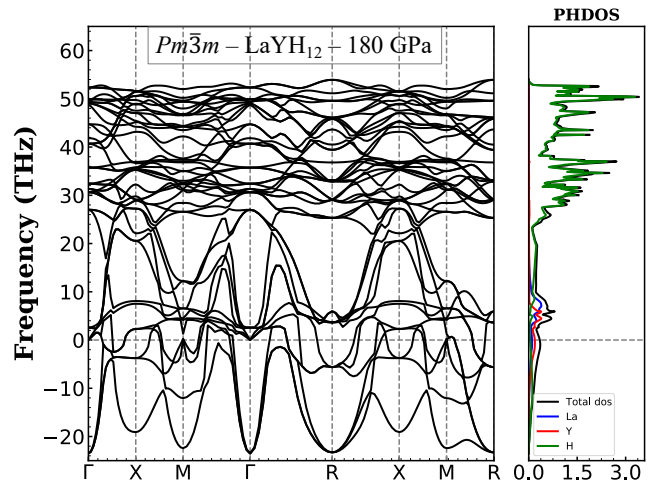


FIG. 5. Phonon dispersions and projected phonon densities of states for $Pm\bar{3}m$ - LaYH_{12} at 180 GPa.

showing considerably similar X-ray diffraction (XRD) peak patterns as well as that of $Fd\bar{3}m$, as shown in Fig. 2. Furthermore, the possibility of the structural transition between $Cmmm$ and $Pm\bar{3}m$ at higher temperatures is pointed out. [12]

IV. CONCLUSION

In summary, we investigated the possible crystal structures for $(\text{LaH}_6)(\text{YH}_6)_y$ compounds as candidates for forming ternary hydrides to achieve a high T_c using a generic algorithm implemented in USPEX. We determined the thermal stabilities at $y = 1$ (LaYH_{12}) and $y = 3$ ($\text{LaY}_3\text{H}_{24}$). A recently reported structure, $Pm\bar{3}m$, appeared unstable toward the decomposition, i.e., LaYH_{12} ($Pm\bar{3}m$) \rightarrow LaH_6 ($R\bar{3}c$) + YH_6 ($Im\bar{3}m$). However, we discovered other new stable structures that did not exhibit decomposition, namely $Cmmm$ - LaYH_{12} , $R\bar{3}c$ - LaYH_{12} , $Cmmm$ - $\text{LaY}_3\text{H}_{24}$, and $R\bar{3}$ - $\text{LaY}_3\text{H}_{24}$. Among these, the compounds with $Cmmm$ clathrate structures exhibited a $T_c \sim 130$ [K] at approximately $P = 200$ GPa, as estimated using the Allen–Dynes formalism.

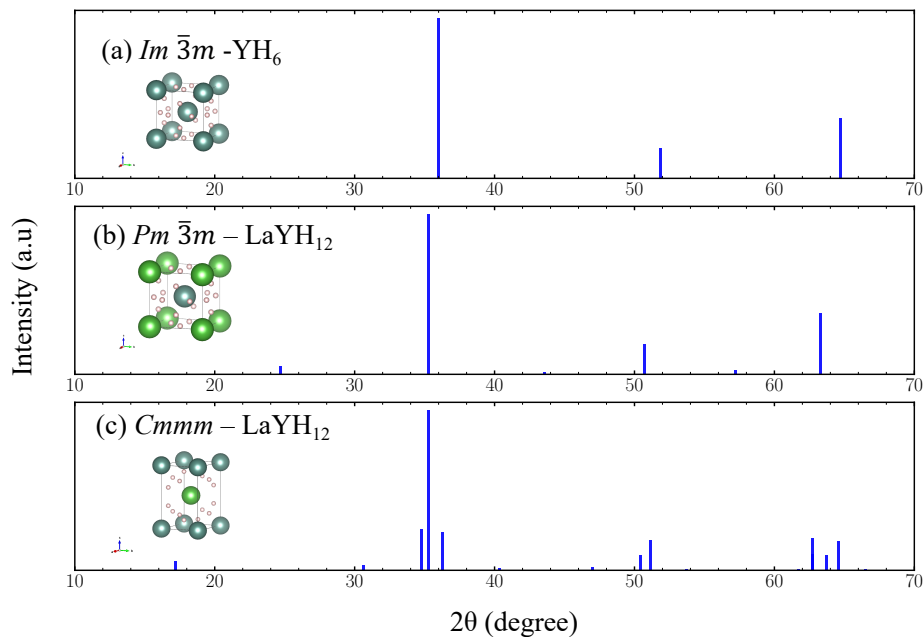


FIG. 6. Structures and the XRD patterns of (a) $Im\bar{3}m$ - YH_6 , (b) $Pm\bar{3}m$ - $LaYH_{12}$, and (c) $Cmmm$ - $LaYH_{12}$.

V. METHODS

For the structural predictions, we used the USPEX code [7] combined with the *ab initio* kernel in the Vienna *ab initio* simulation package (VASP). [49–52] For example, the $LaYH_{12}$ composition randomly generated 400 structures ranging from monomers to tetramers with a $LaYH_{12}$ unit as the “initial generation.” Each generation evolved 100 structures with 40% heredity, 40% randomness, 10% softmutation, and 10% transmutation. When no further evolution occurred for more than 10 generations, the final structure was identified as the candidate crystal structure of the composition. For the identified candidates, we performed *ab initio* geometrical optimizations using the Perdew–Burke–Ernzerhof (GGA–PBE) functional for the exchange–correlation functional. [53]

For the most stable candidates [$R\bar{3}c$ (100–140 GPa) and $Cmmm$ (140–300 GPa) of $LaYH_{12}$, for example], we performed *ab initio* phonon calculations to evaluate their structural stabilities and T_c using the Allen–Dynes formalism, [46–48] implemented in Quantum Espresso. [46] Computational conditions such as the cutoff energy of the plane wave ba-

sis set, sizes of the grid-mesh over the Brillouin zone *etc.* were determined such that the energies sufficiently converged in their dependences. We finally used an $8 \times 8 \times 5$ k -mesh used in the self-consistent field convergence assisted by the Marzari–Vanderbilt smearing scheme. [54] The final energy values were estimated through extrapolation of the smearing parameter toward zero. Mesh sizes for the phonon calculations were $16 \times 16 \times 10$ for the k - and $4 \times 4 \times 2$ for the q -mesh.

VI. ACKNOWLEDGMENTS

The computations in this work have been performed using the facilities of Research Center for Advanced Computing Infrastructure (RCACI) at JAIST. K.H. is grateful for financial support from the HPCI System Research Project (Project ID: hp190169) and MEXT-KAKENHI (JP16H06439, JP17K17762, JP19K05029, and JP19H05169). R.M. is grateful for financial supports from MEXT-KAKENHI (21K03400 and 19H04692), and the Air Force Office of Scientific Research (AFOSR-AOARD/FA2386-17-1-4049;FA2386-19-1-4015)

[1] N. Ashcroft, Phys. Rev. Lett. **92**, 187002 (2004).
 [2] N. W. Ashcroft, Phys. Rev. Lett. **21**, 1748 (1968).
 [3] M. Erements, I. Trojan, S. Medvedev, J. Tse, and Y. Yao, Science **319**, 1506 (2008).
 [4] A. Drozdov, M. Erements, I. Troyan, V. Ksenofontov, and S. I. Shylin, Nature **525**, 73 (2015).

[5] D. Szcześniak and T. Zemła, Supercond. Sci. Technol. **28**, 085018 (2015).
 [6] E. Snider, N. Dasenbrock-Gammon, R. McBride, X. Wang, N. Meyers, K. V. Lawler, E. Zurek, A. Salamat, and R. P. Dias, Phys. Rev. Lett. **126**, 117003 (2021).
 [7] C. W. Glass, A. R. Oganov, and N. Hansen, Comput. Phys. Commun. **175**, 713 (2006).

- [8] Y. Wang, J. Lv, L. Zhu, and Y. Ma, *Comput. Phys. Commun.* **183**, 2063 (2012).
- [9] D. C. Lonie and E. Zurek, *Comput. Phys. Commun.* **182**, 372 (2011).
- [10] F. Peng, Y. Sun, C. J. Pickard, R. J. Needs, Q. Wu, and Y. Ma, *Phys. Rev. Lett.* **119**, 107001 (2017).
- [11] C. Heil, S. Di Cataldo, G. B. Bachelet, and L. Boeri, *Phys. Rev. B* **99**, 220502 (2019).
- [12] Y. Sun, J. Lv, Y. Xie, H. Liu, and Y. Ma, *Phys. Rev. Lett.* **123**, 097001 (2019).
- [13] E. Snider, N. Dasenbrock-Gammon, R. McBride, M. Debessai, H. Vindana, K. Vencatasamy, K. V. Lawler, A. Salamat, and R. P. Dias, *Nature* **586**, 373 (2020).
- [14] Y. Ma, D. Duan, Z. Shao, H. Yu, H. Liu, F. Tian, X. Huang, D. Li, B. Liu, and T. Cui, *Phys. Rev. B* **96**, 144518 (2017).
- [15] Y. Ma, D. Duan, Z. Shao, D. Li, L. Wang, H. Yu, F. Tian, H. Xie, B. Liu, and T. Cui, *Phys. Chem. Chem. Phys.* **19**, 27406 (2017).
- [16] D. Li, Y. Liu, F.-B. Tian, S.-L. Wei, Z. Liu, D.-F. Duan, B.-B. Liu, and T. Cui, *Front. Phys.* **13**, 137107 (2018).
- [17] X. Liang, S. Zhao, C. Shao, A. Bergara, H. Liu, L. Wang, R. Sun, Y. Zhang, Y. Gao, Z. Zhao, *et al.*, *Phys. Rev. B* **100**, 184502 (2019).
- [18] M. Rahm, R. Hoffmann, and N. Ashcroft, *J. Am. Chem. Soc.* **139**, 8740 (2017).
- [19] X. Liang, A. Bergara, L. Wang, B. Wen, Z. Zhao, X.-F. Zhou, J. He, G. Gao, and Y. Tian, *Phys. Rev. B* **99**, 100505 (2019).
- [20] Y. K. Wei, L. Q. Jia, Y. Y. Fang, L. J. Wang, Z. X. Qian, J. N. Yuan, G. Selvaraj, G. F. Ji, and D. Q. Wei, *Int. J. Quantum Chem.*, e26459 (2020).
- [21] H. Xie, D. Duan, Z. Shao, H. Song, Y. Wang, X. Xiao, D. Li, F. Tian, B. Liu, and T. Cui, *J. Phys.: Condens. Matter* **31**, 245404 (2019).
- [22] C. Kokail, W. von der Linden, and L. Boeri, *Phys. Rev. Mater.* **1**, 074803 (2017).
- [23] Z. Shao, D. Duan, Y. Ma, H. Yu, H. Song, H. Xie, D. Li, F. Tian, B. Liu, and T. Cui, *npj Comput. Mater.* **5**, 1 (2019).
- [24] J. Zhang, J. M. McMahon, A. R. Oganov, X. Li, X. Dong, H. Dong, and S. Wang, *Phys. Rev. B* **101**, 134108 (2020).
- [25] P. Zhang, Y. Sun, X. Li, J. Lv, and H. Liu, *Phys. Rev. B* **102**, 184103 (2020).
- [26] S. Di Cataldo, W. von der Linden, and L. Boeri, *Phys. Rev. B* **102**, 014516 (2020).
- [27] X. Guo, R.-L. Wang, H.-L. Chen, W.-C. Lu, K. Ho, and C. Wang, *Phys. Lett. A* **384**, 126189 (2020).
- [28] W. Cui, T. Bi, J. Shi, Y. Li, H. Liu, E. Zurek, and R. J. Hemley, *Phys. Rev. B* **101**, 134504 (2020).
- [29] H.-Y. Lv, S.-Y. Zhang, M.-H. Li, Y.-L. Hai, N. Lu, W.-J. Li, and G.-H. Zhong, *Phys. Chem. Chem. Phys.* **22**, 1069 (2020).
- [30] Y. Yan, T. Bi, N. Geng, X. Wang, and E. Zurek, *J. Phys. Chem. Lett.* **11**, 9629 (2020).
- [31] T. Muramatsu, W. K. Wanene, M. Somayazulu, E. Vinitsky, D. Chandra, T. A. Strobel, V. V. Struzhkin, and R. J. Hemley, *J. Phys. Chem. C* **119**, 18007 (2015).
- [32] D. Meng, M. Sakata, K. Shimizu, Y. Iijima, H. Saitoh, T. Sato, S. Takagi, and S.-i. Orimo, *Phys. Rev. B* **99**, 024508 (2019).
- [33] M. Somayazulu, M. Ahart, A. K. Mishra, Z. M. Geballe, M. Baldini, Y. Meng, V. V. Struzhkin, and R. J. Hemley, *Phys. Rev. Lett.* **122**, 027001 (2019).
- [34] I. Errea, M. Calandra, C. J. Pickard, J. Nelson, R. J. Needs, Y. Li, H. Liu, Y. Zhang, Y. Ma, and F. Mauri, *Phys. Rev. Lett.* **114**, 157004 (2015).
- [35] G. Gao, A. R. Oganov, Y. Ma, H. Wang, P. Li, Y. Li, T. Iitaka, and G. Zou, *J. Chem. Phys.* **133**, 144508 (2010).
- [36] B. Liu, W. Cui, J. Shi, L. Zhu, J. Chen, S. Lin, R. Su, J. Ma, K. Yang, M. Xu, *et al.*, *Phys. Rev. B* **98**, 174101 (2018).
- [37] P.-H. Chang, S. Silayi, D. Papaconstantopoulos, and M. Mehl, *J. Phys. Chem. Solids* **139**, 109315 (2020).
- [38] A. Nakanishi, T. Ishikawa, and K. Shimizu, *J. Phys. Soc. Jpn.* **87**, 124711 (2018).
- [39] W. Sukmas, P. Tsuppayakorn-ae, U. Pinsook, and T. Bovornratanaraks, *J. Alloys Compd.* **849**, 156434 (2020).
- [40] T. Ishikawa, T. Miyake, and K. Shimizu, *Phys. Rev. B* **100**, 174506 (2019).
- [41] P. Song, Z. Hou, P. Castro, K. Nakano, K. Hongo, Y. Takano, and R. Maezono, *arXiv preprint arXiv:2103.00193* (2021).
- [42] D. V. Semenok, I. A. Troyan, A. G. Kvashnin, A. G. Ivanova, M. Hanfland, A. V. Sadakov, O. A. Sobolevskiy, K. S. Pervakov, A. G. Gavriluk, I. S. Lyubutin, *et al.*, *arXiv preprint arXiv:2012.04787* (2020).
- [43] H. Wang, S. T. John, K. Tanaka, T. Iitaka, and Y. Ma, *PNAS* **109**, 6463 (2012).
- [44] X.-h. Wang, F.-w. Zheng, Z.-w. Gu, F.-l. Tan, J.-h. Zhao, C.-l. Liu, C.-w. Sun, J. Liu, and P. Zhang, *ACS Omega* (2021).
- [45] N. P. Salke, M. M. D. Esfahani, Y. Zhang, I. A. Kruglov, J. Zhou, Y. Wang, E. Greenberg, V. B. Prakapenka, J. Liu, A. R. Oganov, *et al.*, *Nat. Commun.* **10**, 1 (2019).
- [46] P. Giannozzi, S. Baroni, N. Bonini, M. Calandra, R. Car, C. Cavazzoni, D. Ceresoli, G. L. Chiarotti, M. Cococcioni, I. Dabo, *et al.*, *J. Phys. Condens. Matter.* **21**, 395502 (2009).
- [47] K. Nakano, K. Hongo, and R. Maezono, *Inorg. Chem.* **56**, 13732 (2017).
- [48] K. Nakano, K. Hongo, and R. Maezono, *Sci. Rep.* **6**, 1 (2016).
- [49] G. Kresse and J. Hafner, *Phys. Rev. B* **47**, 558 (1993).
- [50] G. Kresse and J. Hafner, *Phys. Rev. B* **49**, 14251 (1994).
- [51] G. Kresse and J. Furthmüller, *Comput. Mater. Sci.* **6**, 15 (1996).
- [52] G. Kresse and J. Furthmüller, *Phys. Rev. B* **54**, 11169 (1996).
- [53] J. P. Perdew, K. Burke, and M. Ernzerhof, *Phys. Rev. Lett.* **77**, 3865 (1996).
- [54] N. Marzari, D. Vanderbilt, A. De Vita, and M. Payne, *Phys. Rev. Lett.* **82**, 3296 (1999).

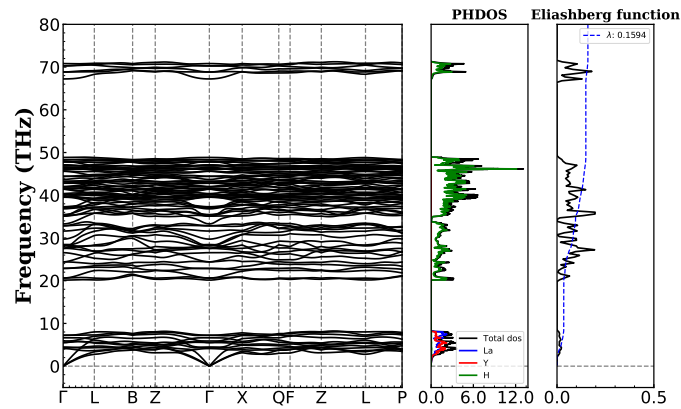
VII. SUPPLEMENTAL INFORMATION

For each compound reported in the main text, we provide the detailed geometries [Table II], Phonon dispersions and Eliashberg spectral functions [Figs. 7-9], and electronic band

structures and Fermi surfaces [Figs. 10-13]. To show the bonding characteristics of the hydrogen atoms in each compound, we also provide the results of the electron localization function (ELF) [Figs. 14 and 15], and the crystal orbital Hamilton population (COHP) [Fig. 16].

TABLE II. Crystal structures of LaYH_{12} and $\text{LaY}_3\text{H}_{24}$ predicted at each pressure (P). Lattice parameters (a , b , and c) are given in units of \AA .

		P (GPa)	Lattice parameters	Atomic coordinates (fractional)			
				Atoms	x	y	z
LaYH_{12}	$R\bar{3}c$	100	$a = b = 5.389$ $c = 13.674$ $\alpha = \beta = 90^\circ$ $\gamma = 120^\circ$	La(6b)	0.00000	0.00000	0.00000
				Y(6a)	0.00000	0.00000	0.25000
				H(36f)	0.00181	0.23464	0.36866
				H(36f)	0.00492	0.27691	0.60940
LaYH_{12}	$Cmmm$	200	$a = 3.617$ $b = 4.956$ $c = 5.156$ $\alpha = \beta = \gamma = 90^\circ$	La(2c)	0.00000	0.50000	0.50000
				Y(2a)	0.00000	0.00000	0.00000
				H(8n)	0.00000	0.11589	0.35519
				H(8n)	0.00000	0.38205	0.11708
				H(8m)	0.25000	0.25000	0.23317
$\text{LaY}_3\text{H}_{24}$	$R\bar{3}$	100	$a = b = 5.324$ $c = 13.569$ $\alpha = \beta = 90^\circ$ $\gamma = 120^\circ$	La(3a)	0.00000	0.00000	0.00000
				Y(6c)	0.00000	0.00000	0.24782
				Y(3b)	0.00000	0.00000	0.50000
				H(18f)	0.00154	0.26668	0.60934
				H(18f)	0.00245	0.23293	0.36741
				H(18f)	0.00465	0.75887	0.87000
				H(18f)	0.01123	0.72593	0.11041
$\text{LaY}_3\text{H}_{24}$	$Cmmm$	180	$a = 3.621$ $b = 5.013$ $c = 10.239$ $\alpha = \beta = \gamma = 90^\circ$	La(2a)	0.00000	0.00000	0.00000
				Y(4l)	0.00000	0.50000	0.25606
				Y(2d)	0.00000	0.00000	0.50000
				H(8n)	0.00000	0.11988	0.19483
				H(8n)	0.00000	0.12176	0.31540
				H(8n)	0.00000	0.37658	0.43798
				H(8n)	0.00000	0.38314	0.07100
				H(8m)	0.25000	0.25000	0.13624
				H(8m)	0.25000	0.25000	0.37798

FIG. 7. Phonon dispersions and projected phonon densities of states for $R\bar{3}c$ - LaYH_{12} clathrate at 100 GPa.

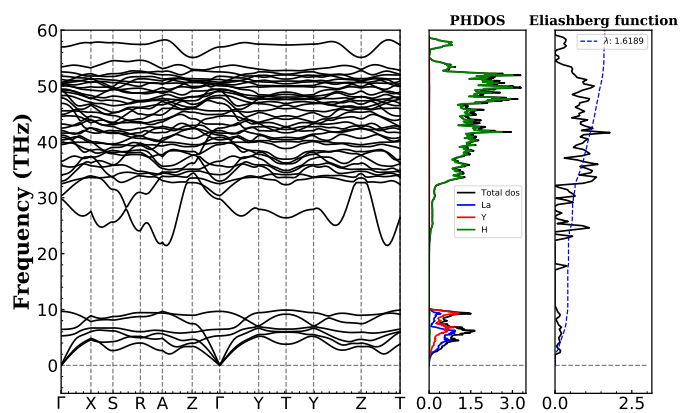


FIG. 8. Phonon dispersions, projected phonon densities of states, and Eliashberg spectral function for $Cmmm$ -LaYH₁₂ clathrate at 250 GPa.

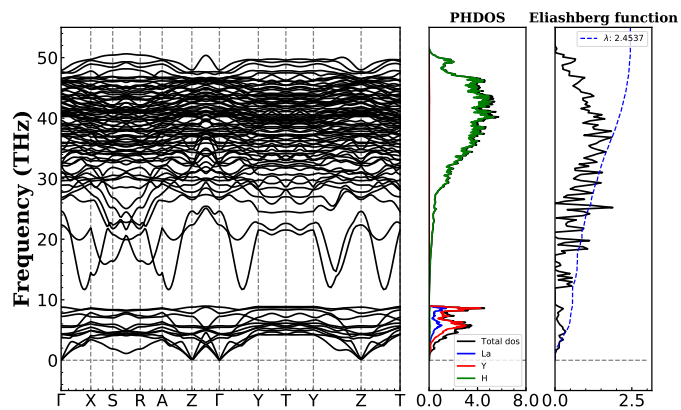


FIG. 9. Phonon dispersions, projected phonon densities of states, and Eliashberg spectral function for $Cmmm$ -LaY₃H₂₄ clathrate at 180 GPa.

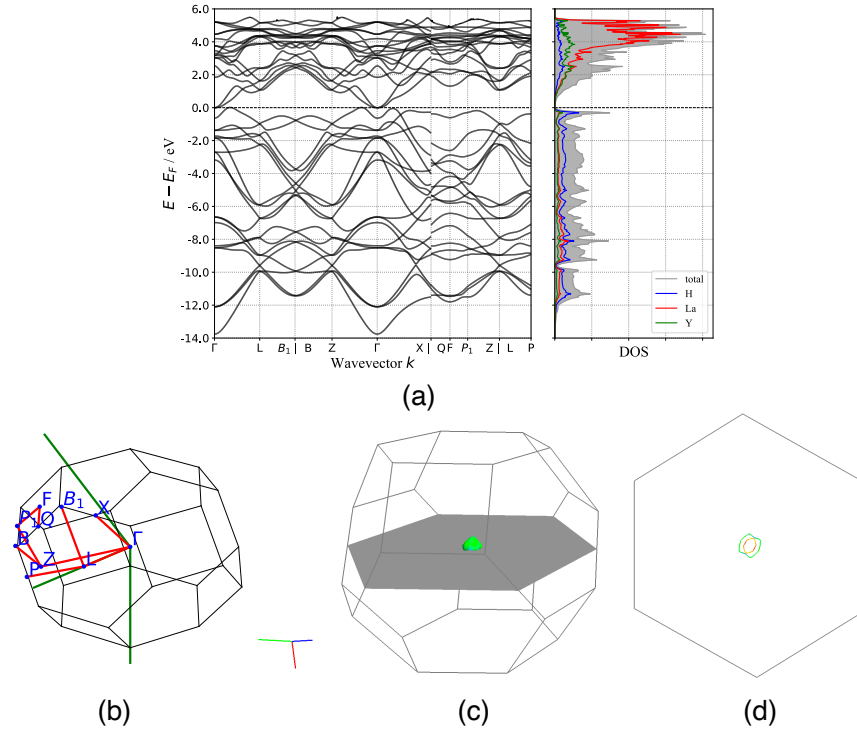


FIG. 10. Band structure, DOS, and Fermi surface of $R\bar{3}c$ -LaYH₁₂.

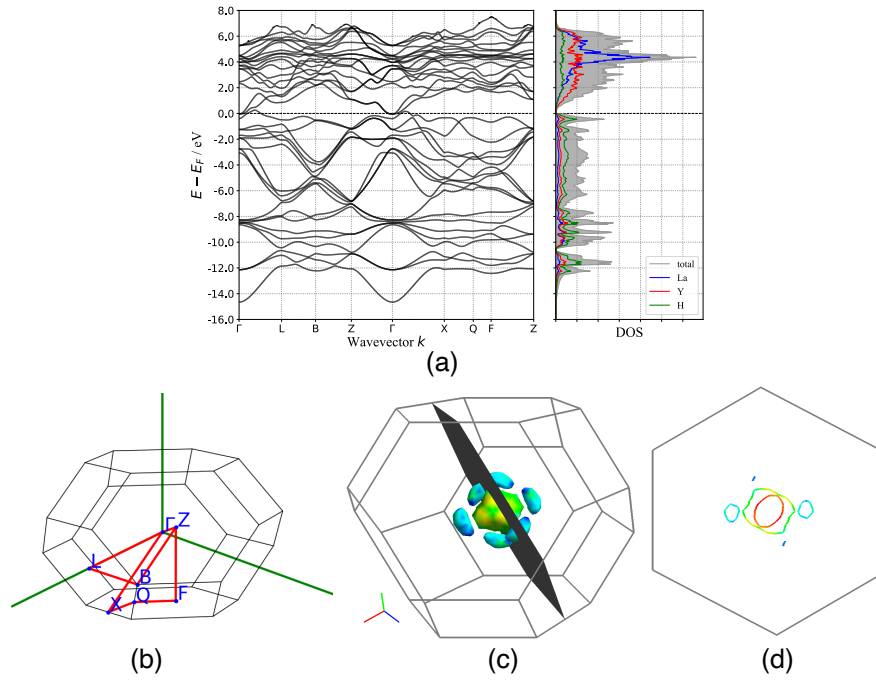


FIG. 11. Band structure, DOS, and Fermi surface of $R\bar{3}$ -LaY₃H₂₄.

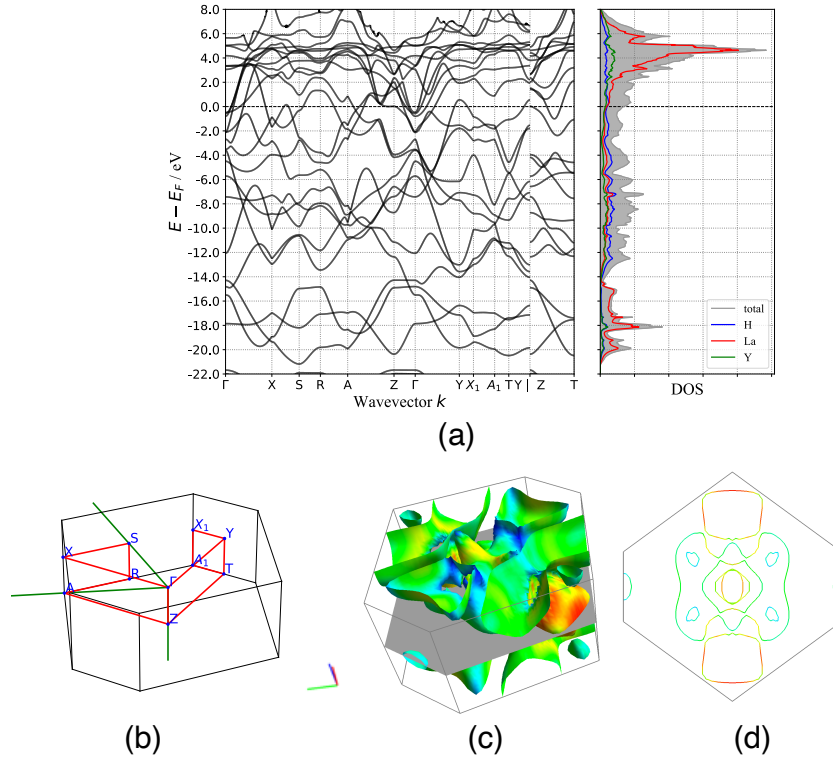


FIG. 12. Band structure, DOS, and Fermi surface of $Cmmm\text{-LaYH}_{12}$

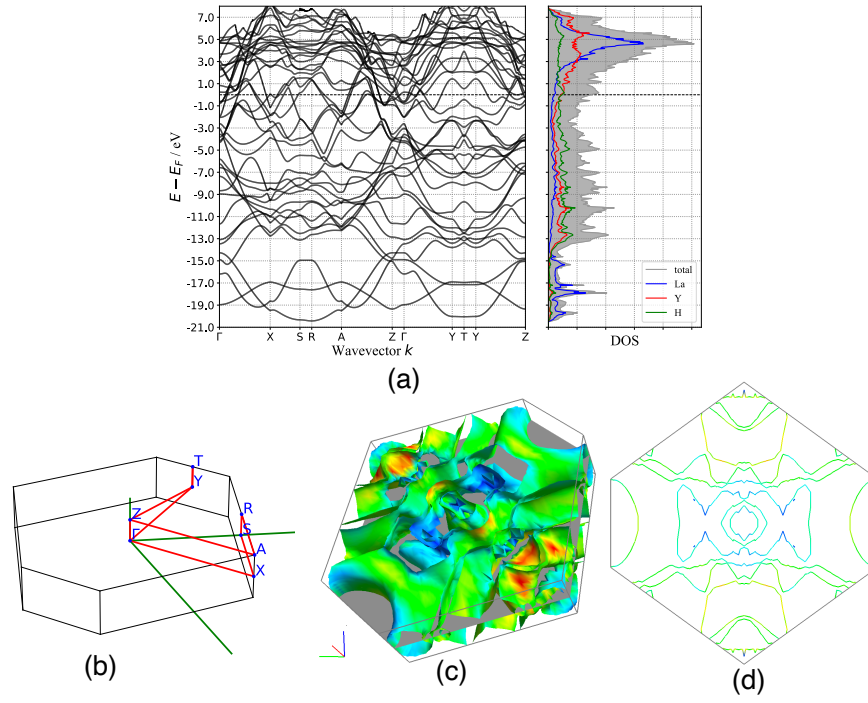


FIG. 13. Band structure, DOS, and Fermi surface of $Cmmm\text{-LaY}_3\text{H}_{24}$

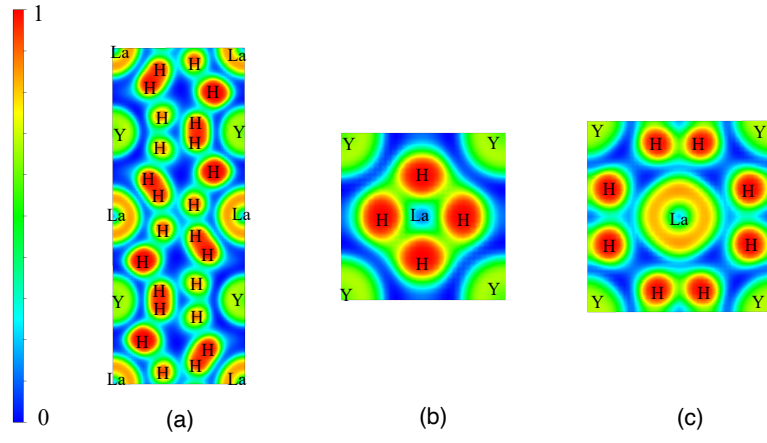


FIG. 14. The calculated ELF of (a) $R\bar{3}c$ -LaYH₁₂, (b) $Pm\bar{3}m$ -LaYH₁₂, and (c) $Cmmm$ -LaYH₁₂ in the (100) plane.

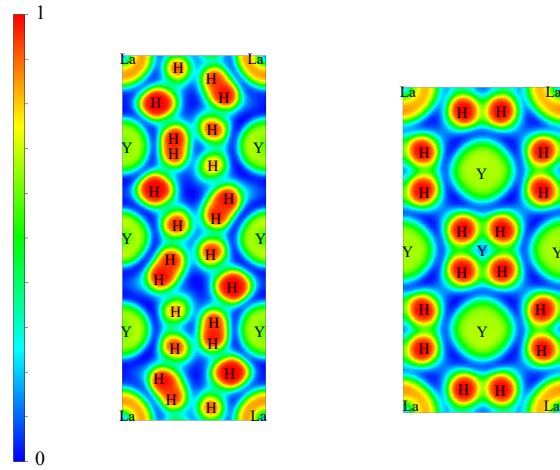


FIG. 15. The calculated ELF of (a) $R\bar{3}$ -LaY₃H₂₄ and (b) $Cmmm$ -LaY₃H₂₄ in the (100) plane.

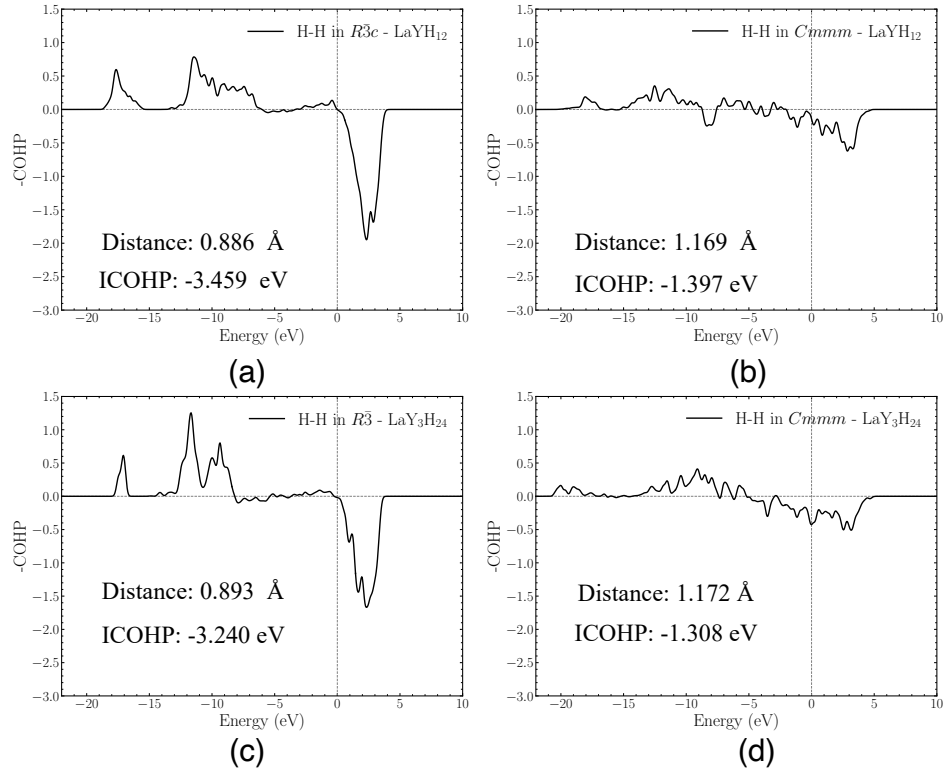


FIG. 16. COHP for pairs of H-H in (a) $R\bar{3}c$ - LaYH_{12} at 100 GPa, (b) $Cmmm$ - LaYH_{12} at 200 GPa, (c) $R\bar{3}$ - $\text{LaY}_3\text{H}_{24}$ at 100 GPa, and (d) $Cmmm$ - $\text{LaY}_3\text{H}_{24}$ at 180 GPa.